

Real space imaging of metastable Bragg glass states in a weakly pinned Type II superconductor

Garima Saraswat^a, Somesh Chandra Ganguli^{a*}, Rini Ganguly^a, Parasharam Shirage^b, Vivas Bagwe^a, Anand Kamlapure^a, Arumugam Thamizhavel^a and Pratap Raychaudhuri^{a†}

^a *Tata Institute of Fundamental Research, Homi Bhabha Road, Colaba, Mumbai 400005, India.*

^b *Indian Institute of Technology Indore, IET-DAVV Campus, Khandwa Road, Indore 452017, India.*

The breakdown of crystalline order in a disordered background connects to some of the most challenging problems in condensed matter physics. For a superconducting vortex lattice, the equilibrium state in the presence of impurities is predicted to be a “Bragg glass” (BG), where the local crystalline order is maintained everywhere and yet the global positional order decays algebraically. Here, using scanning tunnelling spectroscopy (STS) we image the vortex lattice in a weakly pinned NbSe₂ single crystal. We present direct evidence that the ordered state of the VL is a BG, consisting of a large number of degenerate metastable states, which is a hallmark of a glassy state. These results are a significant step towards understanding the disordering of a lattice under the influence of quenched random disorder with a direct impact on various fields, including charge density waves, colloidal crystals and self-organised periodic structures on a substrate.

* e-mail: someshcg@tifr.res.in

† e-mail: pratap@tifr.res.in

I. Introduction

The vortex lattice (VL) in a Type II superconductor provides an ideal system to study various notions related to disordering and melting^{1,2,3}. In a clean superconductor, the VL configuration is determined by two factors: The interaction between vortices which favours their ordering into a hexagonal Abrikosov lattice, and temperature which favours disordering and melts the lattice at a characteristic temperature. Structural imperfections in the superconductor modify this simple scenario by creating a disordered background potential, where the vortices can get pinned at individual defect sites. In the presence of random pinning the VL can no longer support a true long-range order. Of particular interest is the VL state in the presence of weak random pinning well below the locus of the thermodynamic order-disorder transition in magnetic field-temperature (H - T) parameter space. It has been predicted that in equilibrium, the VL exists in a quasi-long-range ordered state, the so called Bragg glass (BG)^{4,5}, where each lattice point maintains six-fold coordination and yet the positional order decays algebraically with distance. The hallmark of such a state is the existence of a large number of degenerate metastable configurations, each with algebraic decay of positional order but different vortex configuration. With increase in temperature/magnetic field this quasi-long-range order is destroyed giving rise to a disordered state⁶.

Both ordered and disordered VL states, as well as order-disorder transitions have been extensively studied through bulk measurements such as critical current^{7,8}, a.c. susceptibility^{9,10,11} and d.c. magnetisation^{12,13}. These studies rely on the fact that in the presence of weak random pinning sites, a disordered VL is more strongly pinned to the crystal than its more ordered counterpart¹⁴. However, a more direct and relatively less explored line of study has been through imaging of the VL in real space^{15,16,17}, which gives direct information on the lattice configuration. Here, using STS down to 350 mK, we image

in real space equilibrium and non-equilibrium states of the VL in a weakly pinned NbSe₂ single crystal, well below the locus^{18,19} of the thermodynamic order-disorder transition (see supplementary information²⁰). We use thermo-magnetic cycling to prepare the VL in a variety of different states, e.g. non-equilibrium disordered states and equilibrium quasi-long range ordered states and use small magnetic pulses to switch between them. Our investigations reveal that while the VL can be prepared both as disordered and quasi-long-range ordered states, the equilibrium state of the system is a BG, composed of large number of degenerate metastable states, which can be accessed using small magnetic perturbations.

II. Experimental Details

NbSe₂ single crystals were grown by iodine vapor transport method, starting with 99.99 % pure Nb powder and 99.999 % Se shots. Stoichiometric amounts of pure Nb and Se, together with iodine as the transport agent were mixed and placed in one end of a quartz tube, which was then evacuated and sealed. The sealed quartz tube was heated up in a temperature gradient furnace for 5 days, with the charge-zone and growth-zone temperatures, 800°C and 720° C respectively. We obtained NbSe₂ single crystals with lateral size 4-5 mm. Resistivity (ρ) measurements showed a superconducting transition temperature, $T_c \sim 7.2$ K with transition width of $\Delta T_c \sim 0.15$ K and a residual resistance ratio $\rho(300\text{ K})/\rho(10\text{ K}) \sim 25$.

The VL is imaged using a home-built scanning tunneling microscope²¹ (STM) operating down to 350 mK and fitted with an axial 9 T superconducting solenoid. Prior to STM measurements, the crystal is cleaved in-situ in vacuum giving atomically smooth facets larger than $1\ \mu\text{m} \times 1\ \mu\text{m}$. Since the vortex core behaves like a normal metal, well resolved images of the VL are obtained by measuring the tunneling conductance, $G(V) = dI/dV$, at a fixed bias voltage (V) on the surface of the superconductor. We fix $V \sim 1.4$ mV, which is close to the superconducting coherence peaks such that each vortex core manifests as a local minimum in $G(V)$. The precise position of the vortices are obtained from the images after

digitally removing scan lines and finding the local minima in $G(V)$ using WSxM software²². Each image contains between 250-380 vortices. To identify topological defects, we Delaunay triangulate the VL and determine the nearest neighbor coordination for each flux lines. Topological defects in the hexagonal lattice manifest as points with 5-fold or 7-fold coordination number. The bulk pinning property of the VL is measured on the same crystal from the real part of a. c. susceptibility (χ') using a home built susceptometer.

III. Results and Discussion

We first show the bulk pinning properties (Fig. 1) of the VL at 15 kOe created using different field cooling protocols, measured from the temperature variation of χ' . The two primary states are the zero field cooled (ZFC) state (where the sample is cooled to the lowest temperature in zero field and subsequently a magnetic field is applied) exhibiting weakest pinning and the field cooled (FC) state (where the field is applied at $T > T_c$ and the sample is cooled in the presence of magnetic field) exhibiting strongest pinning. The ZFC state shows a diffuse “peak effect” at $T_p \sim 4.6$ K (Fig. 1(b)), indicating that the sample is moderately disordered¹⁰. A number of intermediate states with progressively increasing pinning can be accessed by first preparing the VL using the ZFC protocol, and then heating the sample to a higher temperature T^* ($< T_c$) and cooling back (Fig. 1(a)). We observe that when the FC VL is shaken by applying a small magnetic pulse of 130 Oe (Fig. 1(b)), the VL undergoes a dynamic transition to a state very close to the ZFC state, and after four successive pulses it becomes indistinguishable from the ZFC state. On the other hand, the bulk pinning response of the ZFC state remains unaltered with application of field pulses, which confirms that the ZFC state is the equilibrium state of the system.

Fig. 2(a) and 2(b) show the real space VL image over an area of 500×500 nm, for the ZFC and FC state at 15 kOe and 350 mK. By analyzing the Delaunay triangulation of the

structures we observe that the ZFC state is free from topological defects. The vortex lattice constant, $a \approx 39.8$ nm, is in excellent agreement with expected value at 15 kOe. In contrast, we identify three dislocation pairs in the FC lattice within the field of view. When the FC lattice is shaken with a magnetic field pulse of 100 Oe two of the three dislocations are annihilated (Fig. 2(c)). Repeating this experiment with a pulse of 130 Oe we observe that all dislocations are annihilated resulting in state similar to the ZFC state (Fig. 2(d)).

In order to analyze the VL images more quantitatively we calculate the orientational and positional correlation functions, $G_6(\bar{r})$ and $G_{\bar{K}}(\bar{r})$, which measure the degree of misalignment and the relative displacement between two vortices separated by distance r respectively, with respect to the lattice vector of an ideal hexagonal lattice. The orientational correlation function is defined as, $G_6(r) = \langle \cos 6(\theta(\bar{r})) \rangle$, where $\theta(\bar{r})$ is the angle between the bond located at origin and the bond located at position \bar{r} . We calculate $G_6(r)$ by evaluating the average, $\frac{1}{n(r)} \sum_r^{r+\delta r} \cos 6(\theta(\bar{r}))$, over a circular shell containing $n(r)$ bonds at distance r from the origin, and further averaging over this quantity calculated by shifting the origin over the mid-point of each of the bonds in the lattice²³. The spatial correlation function, $G_{\bar{K}}(r) = \langle \cos \bar{K} \cdot \bar{r} \rangle$, (where r is the position of the vortex and \bar{K} is the reciprocal lattice vector obtained from the Fourier transform) is calculated from the position of the vortices using a similar averaging procedure²⁴. For an ideal hexagonal lattice both $G_6(r)$ and $G_{\bar{K}}(r)$ are 1 for all values of r .

Fig. 3(a) and (b) show $G_6(r)$ and $G_{\bar{K}}(r)$ respectively for the states corresponding to Fig. 2(a)-(d). For both the states containing dislocations, i.e. the FC state, and the partially healed FC state after applying a pulse of 100 Oe, $G_{\bar{K}}(r) \propto e^{-r/L}$ with a decay length of $L \approx 4.49a$ and $L \approx 5.09a$ respectively (Fig. 3(c)) and $G_6(r)$ decay as a power-law (Fig. 3(d)).

These are characteristic of a hexatic state with short range positional order but quasi long range orientational order²⁵. In contrast, for the ZFC state and the healed FC state after applying a pulse of 130 Oe, $G_{\bar{k}}(r) \propto 1/r^n$ (Fig. 3(e)) and $G_6(r)$ reach a constant value ~ 0.845 after 1.5 lattice constant (Fig. 3(f)). This is consistent with long range orientational order and a quasi-long range positional order expected for a BG^{26,27}. We confirmed that the intermediate states shown in Fig. 1(a), are similar to the FC state but containing different density of topological defects.

We now address the central issue concerning the glassiness in the BG state. Since a glassy state is expected to contain many degenerate metastable states with same degree of positional order, perturbing the equilibrium BG state, one would expect to switch between these states. To verify this, we prepare the VL in the ZFC state and shake the lattice with a series of 130 Oe magnetic field pulses. While the VL images obtained after applying successive pulses (Fig. 4(a)-(d)) show that they are free from topological defects, after each pulse the VL configuration is different. The difference between successive images (after subtracting the mean value of the conductance over the entire area and normalising the amplitude of the vortex signal to one) is shown in Fig. 4(e)-(g). The difference between the image before and after each pulse shows that after each pulse the VL in some parts of the image drastically rearrange, whereas in other parts it remains relatively unchanged. We have independently verified that the lateral drift in our STM is well below 0.5 nm, such that the same area is imaged in each of these scans. Fig. 4(h) and (i) show the $G_6(r)$ and $G_{\bar{k}}(r)$ respectively corresponding to the images in Fig. 4(a)-(d). The radial decay of $G_6(r)$ and $G_{\bar{k}}(r)$ for each of these states is similar and characteristic of a Bragg glass. Thus after each pulse we realise a different metastable realisation of the equilibrium BG state having the same degree of positional and orientational order.

IV. Summary

In summary, we have shown that in the presence of weak random pinning, the equilibrium VL state below the thermodynamic order-disorder transition is quasi-long-range ordered BG, composed of a large number of metastable states, each characterised by the absence of topological disorder and an algebraic decay of the positional correlation. We also show that dislocations in a disordered vortex lattice can be gradually annealed by shaking the lattice with small magnetic field pulses, thus driving it into a BG state. These results are directly relevant to design strategies for growing large self-assembled periodic structures on a substrate^{28,29,30}, a field of great contemporary interest in material science and photonics³¹, where the main challenge is to extend the defect free structure over large length scales. It would be instructive to study the evolution of the BG state as a function of pinning strength, and find the critical value at which the equilibrium state of the system is driven into disordered vortex glass. Such experiments could be performed on colloidal crystals in random optical traps where the strength the pinning potential can be tuned by the strength of optical field, and would provide further insight on the role of random pinning on the crystalline state.

Acknowledgements

The authors thank Shobo Bhattacharya, Arun Kumar Grover, Srinivasan Ramakrishnan and Deepak Dhar for illuminating discussions during the course of the work. The work was funded by Department of Atomic Energy, Government of India. PS acknowledges Department of Science and Technology, Government of India for partial financial support through grant no SR/S2/RF-121/2012.

-
- ¹M. J. Higgins and S. Bhattacharya, *Physica C* **257**, 232(1996).
- ²G. Blatter, M. V. Feigel'man, V. B. Geshkenbein, A. I. Larkin and V. M. Vinokur, *Rev. Mod. Phys.* **66**, 1125 (1994).
- ³Y. Paltiel, E. Zeldov, Y. N. Myasoedov, H. Shtrikman, S. Bhattacharya, M. J. Higgins, Z. L. Xiao, E. Y. Andrei, P. L. Gammel and D. J. Bishop, *Nature* **403**, 398 (2000).
- ⁴T. Giamarchi and P. Le Doussal, *Phys. Rev. B* **52**, 1242 (1995).
- ⁵T. Klein, I. Joumard, S. Blanchard, J. Markus, R. Cubitt, T. Giamarchi and P. Le Dousal, *Nature* **413**, 404 (2001).
- ⁶D. S.Fisher, M. P. A.Fisher and D. A. Huse, *Phys. Rev. B* **43**, 130 (1991).
- ⁷W. Henderson, E. Y. Andrei, M. J. Higgins and S. Bhattacharya, *Phys. Rev. Lett.* **77**, 2077 (1996).
- ⁸S. Mohan, J. Sinha, S. S. Banerjee, A. K. Sood, S. Ramakrishnan and A. K. Grover, *Phys. Rev. Lett.* **103**, 167001 (2009).
- ⁹K. Ghosh, S. Ramakrishnan, A. K. Grover, G. I. Menon, G. Chandra, T. V. Chandrasekhar Rao, G. Ravikumar, P. K. Mishra, V. C. Sahni, C. V. Tomy, G. Balakrishnan, D.Mck Paul and S. Bhattacharya, *Phys. Rev. Lett.* **76**, 4600 (1996).
- ¹⁰S. S. Banerjee, N. G. Patil, S. Ramakrishnan, A. K. Grover, S. Bhattacharya, G. Ravikumar, P. K. Mishra, T. V. Chandrasekhar Rao, V. C. Sahni and M. J. Higgins, *Appl. Phys. Lett.* **74**, 126 (1999).
- ¹¹G. Pasquini, D. Pérez Daroca, C. Chliotte, G. S. Lozano and V. Bekeris, *Phys. Rev. Lett.* **100**, 247003 (2008).
- ¹²G. Ravikumar, V. C. Sahni, A. K. Grover, S. Ramakrishnan, P. L. Gammel, D. J. Bishop, E. Bucher, M. J. Higgins and S. Bhattacharya, *Phys. Rev. B* **63**, 024505 (2000).
- ¹³H. Pastoriza, M. F. Goffman, A. Arribére and F. de la Cruz, *Phys. Rev. Lett.* **72**, 2951 (1994).
- ¹⁴A. Larkin and Y. Ovchinnikov, *J. Low Temp. Phys.* **34**, 409 (1979).
- ¹⁵A. M. Troyanovski, M.van Hecke, N. Saha, J. Aarts and P. H. Kes, *Phys. Rev. Lett.* **89**, 147006 (2002).
- ¹⁶A. P. Petrović, Y. Fasano, R. Lortz, C. Senatore, A. Demuer, A. B. Antunes, A. Paré, D. Salloum, P. Gougeon, M. Potel and Ø. Fischer, *Phys. Rev. Lett.* **103**, 257001 (2009).
- ¹⁷I. Guillamón, H. Suderow, A. Fernández-Pacheco, J. Sesé, R. Córdoba, J. M. De Teresa, M. R. Ibarra and S.Vieira, *Nature Physics* **5**, 651 (2009).

-
- ¹⁸S. S.Banerjee, N. G.Patil, S. Ramakrishnan, A. K. Grover, S. Bhattacharya, P. K. Mishra, G. Ravikumar, T. V. Chandrasekhar Rao, V. C. Sahni, M. J. Higgins, C. V. Tomy, G. Balakrishnan and D. Mck. Paul, Phys. Rev. B **59**, 6043 (1999).
- ¹⁹A. D. Thakur, T. V. Chandrasekhar Rao, S.Uji, T. Terashima, M. J. Higgins, S. Ramakrishnan and A. K. Grover, J. Phys. Soc. Jpn. **75**, 074718 (2006).
- ²⁰See Supplemental Material at [*URL will be inserted by publisher*] for thermodynamic order-disorder transition driven by magnetic field at 350 mK.
- ²¹A. Kamlapure, G. Saraswat, S. C. Ganguli, V. Bagwe, P. Raychaudhuri and S. P. Pai, Rev. Sci. Instrum. **84**, 123905 (2013).
- ²²I. Horcas, R. Fernández, J. M.Gómez-Rodríguez, J. Colchero, J. Gómez-Herrero and A. M. Baro, Rev. Sci. Instrum. **78**, 013705 (2007).
- ²³R. A. Quinn, C. Cui, J. Goree, J. B. Pieper, H. Thomas and G. E. Morfill, Phys. Rev. E **53**, R2049 (1996).
- ²⁴Y. Fasano and M. Menghini, Supercond. Sci. Technol. **21**, 023001(2008).
- ²⁵J. M. Kosterlitz and D. J. Thouless, ed. Jorge V Jose (World Scientific, 2013).
- ²⁶T. Nattermann, Phys. Rev. Lett. **64**, 2454 (1990).
- ²⁷T. Giamarchi and P. le Doussal, Phys. Rev. Lett **72**, 1530 (1994).
- ²⁸A. M.Alsayed, M. F. Islam, J. Zhang, P. J. Collings and A. G. Yodh, Science **309**, 1207 (2005).
- ²⁹P. Pieranski, L. Strzelecki and B. Pansu, Phys. Rev. Lett. **50**, 900 (1983).
- ³⁰T. Zhang, X. Tuo and J. Yuan, Langmuir **25**, 820 (2009).
- ³¹J. F. Galisteo-López, M. Ibisate, R. Sapienza, L. S. Froufe-Pérez, Á. Blanco and C. López, Adv. Mater. **23**, 30 (2011).

Figure Captions:

Figure 1. (a) χ' vs. T at 15 kOe for the VL prepared using different protocols. (b) χ' vs. T for the ZFC and FC states and after applying different number of magnetic field pulses of 130 Oe on the FC state. χ' is normalised to zero field value at lowest temperature. The data is recorded while heating the sample.

Figure 2. Real space image (500×500 nm) of the VL at 350 mK in magnetic field of 15 kOe after preparing the VL using different protocols: (a) ZFC, (b) FC, (c) after applying a pulse of 100 Oe and (d) after applying a pulse of 130 Oe on the FC state. The lines show Delaunay triangulation and the dislocations in the VL are shown as pairs of points with five-fold (red) and seven-fold (white) coordination. Corresponding Fourier transforms are shown on the right panel of each real space image.

Figure 3. (a) Orientational correlation function, G_6 and (b) and positional correlation function, G_k (averaged over the principal symmetry directions) as a function of r/a for the VL configurations shown in Fig. 2(a)-(d). a is calculated by averaging over all the bonds after Delaunay triangulating the image. G_k and G_6 for the FC state and with the 100 Oe pulse: (c) G_k is plotted in semi-log scale showing the exponential decay, and (d) G_6 is plotted in log-log scale showing power law decay. G_k and G_6 for ZFC and 130 Oe pulse: (e) G_k is plotted in log-log scale showing power law decay, (f) an expanded view showing that G_6 is constant ~ 0.845 (red line) after 2 lattice constants. The black lines in panels (c)-(e) show the fit to the exponential/power-law decay respectively.

Figure 4. Real space image (670×670 nm) at 350 mK of (a) the ZFC VL at 15 kOe and (b)-(d) after applying successive magnetic field pulses of 130 Oe. Delaunay triangulations of the

VL are shown in the same figures. After each pulse the VL configuration is altered which is apparent from the difference between images before and after each pulse: (e) (b)-(a) (f) (c)-(b) and (g) (d)-(c). (h) Orientational correlation function, G_6 and (i) positional correlation function, G_k (averaged over the principal symmetry directions) as a function of r/a for the VL configurations shown in panels (a)-(d).

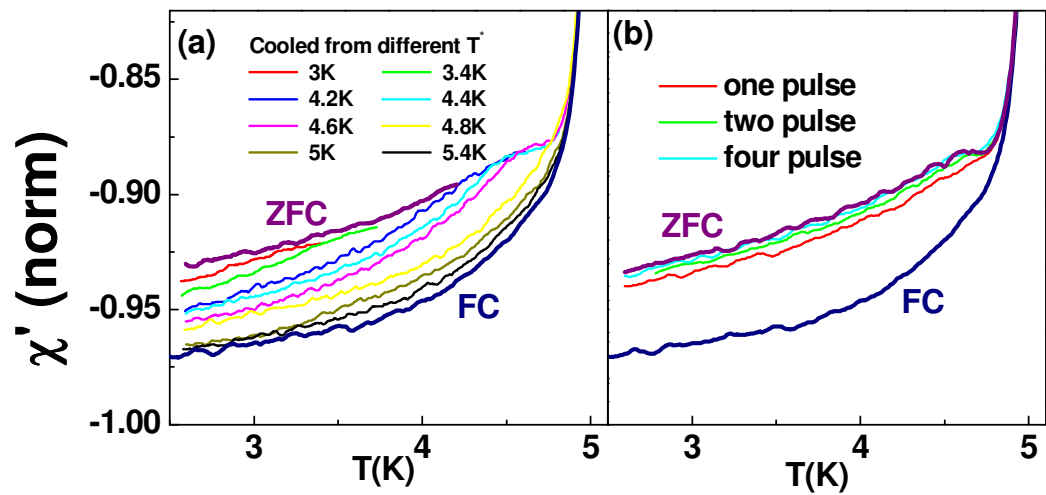


Figure 1

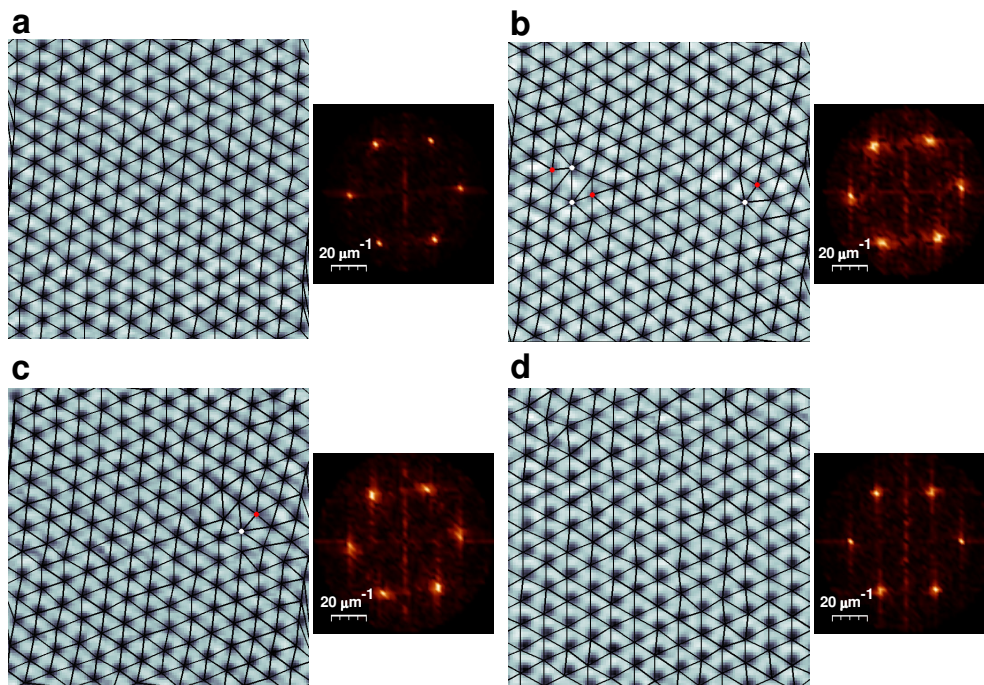


Figure 2

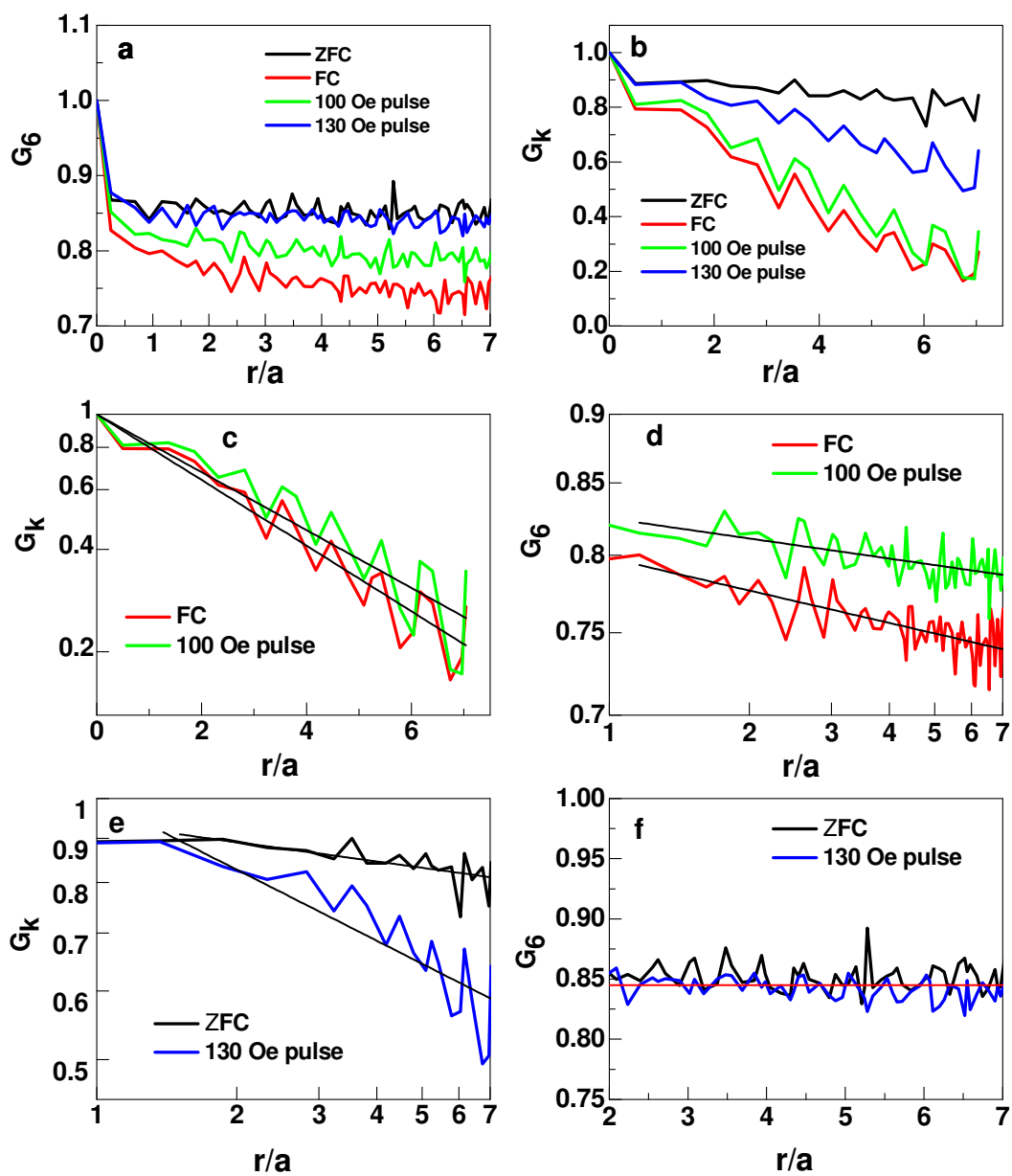


Figure 3

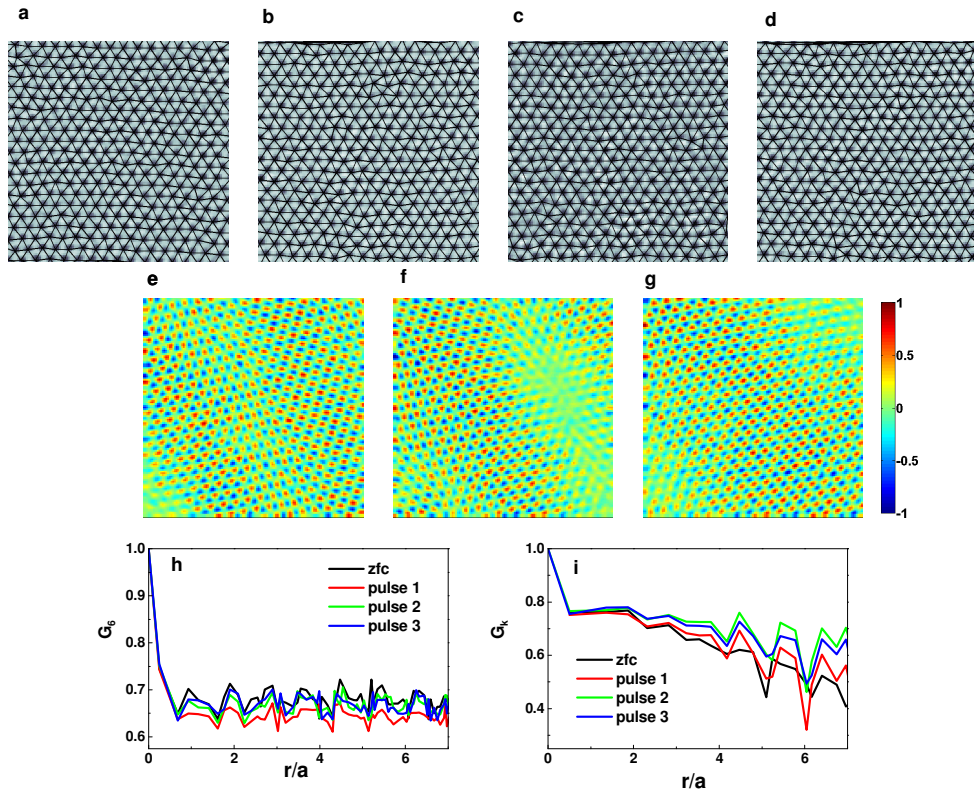


Figure 4